Journal of Ambient Intelligence and Humanized Computing (2020) 11:4983–4994
https://doi.org/10.1007/s12652-020-01777-7

ORIGINAL RESEARCH

A fuzzy adaptive gravitational search algorithm for two-dimensional multilevel thresholding image segmentation

Zhiping Tan[1] · Dongbo Zhang[2]

Received: 6 September 2019 / Accepted: 6 February 2020 / Published online: 19 February 2020

Abstract
Two-dimensional (2D) multilevel thresholding is an important technique for noisy image segmentation which has drawn much attention during the past few years. The conventional image segmentation methods are efficient for 2D bi-level thresholding. However, the computational complexity grows exponentially when extended to 2D multilevel thresholding since they search the optimal thresholds by exhaustive strategy. To tackle this problem, a fuzzy adaptive gravitational search algorithm (FAGSA) using Tsallis entropy as its objective function has been presented to find the optimal 2D multilevel thresholds in this paper. In the FAGSA, fuzzy logic controllers are designed to tune the control parameters. The state-of-the-art heuristic algorithms are compared with this proposed algorithm. Both test images and noisy images are utilized in the experiments to evaluate the performance of the involved algorithms. The experimental results significantly demonstrate the superiority of our algorithm in terms of the objective function value, image quality measures and time consumption.

Keywords Image segmentation · Two-dimension multilevel thresholding · Fuzzy adaptive gravitational search algorithm · Tsallis entropy

1 Introduction

Image segmentation refers to dividing an image into object and background which is widely used in image processing and computer vision (Chen et al. 2017). In the past few decades, many image segmentation approaches have been proposed and applied in various fields (Zeng et al. 2016; Badrinarayanan et al. 2017). Thresholding often provides an easy and convenient way to isolate objects of interest from the background which becomes a popular image segmentation technique (Cheriet et al. 1998). At present, thresholding segmentation contains bi-level and multi-level (El Aziz et al. 2017). Bi-level thresholding segments an image into two different parts. However, if an image is composed of several distinct objects, multilevel thresholds may obtain the desirable result. In generally, thresholding segmentation methods are almost based on one-dimensional histograms (Li and Tan 2019), but the spatial correlation among pixels is not taken into account, the performance of the method in noisy images is not satisfactory (Sha et al. 2016), for this reason, the 2D histogram is conceived (Abdel-Khalek et al. 2017). Subsequently, 2D multilevel thresholding image segmentation method is proposed (Ishak 2017b, a). However, the computation time is expensive when exhaustively searching multilevel thresholds. Hence, finding the optimal 2D multilevel thresholding is a challenging task (Ishak 2017b, a). The multilevel thresholding is difficult to get satisfying answer in reasonable time by conventional mathematical deterministic methods. This is an NP-hard combinational optimization problem (Khairuzzaman and Chaudhury 2017). In such case, meta-heuristic methods attracted much attention in recent years (Zeng et al. 2018). Most of the related works are based on swarm-intelligence, such as particle swarm optimization (PSO) (Xiong et al. 2019a) and the extraction algorithm of color disease (Xiong et al. 2019b), differential evolution (DE) (Sarkar et al. 2015), artificial bee colony (ABC) (Horng 2011), harmony search algorithm (HSA) (Erwin and Saputri 2018), firefly algorithm (FA) (Pare et al. 2018),

✉ Dongbo Zhang
dongbozhang2013@qq.com

Zhiping Tan
tzp2008ok@163.com

[1] College of Mathematics and Informatics, South China Agricultural University, Guangzhou 510642, China

[2] Guangdong Key Laboratory of Modern Control Technology, Guangdong Institute of Intelligent Manufacturing, Guangzhou 510070, China

cuckoo search (CS) (Bhandari et al. 2014), gravitational search algorithm (GSA) (Rashedi et al. 2009), bat algorithm (BA) (Gandomi et al. 2013), flower pollination algorithm (FPA) (Bhandari et al. 2016). Moreover, amount of modified and improved meta-heuristic algorithms are applied to multilevel thresholding (He and Huang 2017; Bhandari et al. 2015).

GSA is an optimization method inspired by the theory of Newtonian gravity in physics (Duman et al. 2012). Recently, GSA has been applied to several areas with promising performances feature selection (Nagpal et al. 2017), numerical optimization (Sarafrazi et al. 2015), power systems (Beigvand et al. 2016), multi-objective optimization and so on (Sun et al. 2016). The studies show that the GSA is remarkably promising and could outperform the other well known algorithms. The success recorded by the GSA is attributed to its striking balance between local and global searching. In addition, the fewer number of parameters required by the GSA for execution (Yazdani et al. 2014). However, although the GSA have been well-applied for solving many problems, but when dealing with different optimization problems, the GSA need to adjust the control parameters, and adopt new operators to enhance the performance (Kumar and Sahoo 2014). Nobahari et al. (2012) modeled two mutation operators in GSA, called sign and reordering, to improve the diversity of the population. Han and Chang (2012) applied a novel chaotic operator in GSA to overcome premature convergence and to avoid falling into local minima Rashedi et al. (2009). presented a clustering algorithm for image segmentation motivated by GSA equipped with a new operator, called escape. Doraghinejad and Nezamabadi-pour (2014) proposed a black hole operator strategy, which provoked by some characteristics of the black hole phenomenon in astronomy. The original GSA can be divided into two categories according to kinds of parameter control and hybridization. Parameters can be controlled, deterministic, adaptive and self-adaptive. Hybridization means incorporating the problem-specific knowledge into the original optimization algorithm (Kang et al. 2018; Sun et al. 2018). In summary, all the operations are utilized to balance the exploration and exploitation (Rashedi et al. 2018).

In order to enhance the stability and robustness of the GSA, a new approach FAGSA has been proposed for selecting the 2D multilevel thresholds. In our work, we took the Tsallis entropy as the measure. Our objective is to segment the image by maximizing the 2D Tsallis entropy. The optimization task will be accomplished using FAGSA. Indeed, the main object of this study is to demonstrate the effectiveness of the proposed algorithm, especially on multimodal images and noisy images.

The remainder of this paper is organized as follows. First, Sect. 2 exposes the employed Tsallis entropy and the two dimensional multilevel thresholding in details. The FAGSA will be described in Sect. 3. In Sect. 4, the performance of the proposed algorithm is evaluated by performing a series of test images. Section 5, some conclusions are drawn.

2 Two-dimensional multilevel thresholding model

In this section, the two-dimensional multilevel thresholding method for image segmentation is proposed. We introduce the concept of the Tsallis entropy and two-dimensional histogram computation and the two dimensional Tsallis entropy.

2.1 Tsallis entropy

Entropy is basically a thermodynamic concept associated with the order of irreversible processes from a traditional point of view. The seminal work of Shannon initiated the area of research now known as information theory. Shannon states that the great deal of information $S(A)$ contained in a system A of N events with probabilities $P_i=P_1, P_2,\ldots, P_N, \sum_{i=1}^{N} P_i = 1$, can be measured by:

$$S(A) = -\sum_{i=1}^{N} P_i \ln P_i \tag{1}$$

This quantity has since become known as the Shannon entropy which has been widely used in different fields. Extensions of Shannon's original work have resulted in many alternative measures of information. Tsallis proposed a non-extensive entropy based on the Shannon entropy which can be defined as (Raja et al. 2018):

$$T_q(A) = \frac{1 - \sum_{i=1}^{N} P_i^q}{q-1} \tag{2}$$

where q is an entropic index, generally $q=0.8$. For two independent subsystems A_1 and A_2, on account of pseudo additive rule, the total Tsallis entropy of the system satisfies the following equation:

$$T_q(A_1 + A_2) = T_q(A_1) + T_q(A_2) + (1-q)\cdot T_q(A_1)\cdot T_q(A_2) \tag{3}$$

Based on multi-fractal theory, the generalization of the pseudo additive rule can be extend to $m+1$ independent subsystems $A_1, A_2,\ldots, A_{k+1}$ takes the following form:

$$\begin{aligned} T_q(A_1 + A_2 + \cdots + A_{m+1}) = &\sum_{i=1}^{m+1} T_q(A_i) + (1-q)\sum_{i\neq j} T_q(A_i)T_q(A_j) \\ &+(1-q)^2 \sum_{i\neq j\neq r} T_q(A_i)T_q(A_j)T_q(A_r) \\ &+\cdots+(1-q)^m \prod_{i=1}^{m+1} T_q(A_i) \end{aligned} \tag{4}$$

2.2 2D histogram computations

For an image with L gray-levels, $\{L|L=1,2,\ldots,256\}$, and let $U=\{u_1,\ldots,u_L\}$ be the ordered set of all the gray-levels (u_1 and u_L are respectively the minimum and maximum gray values). A digital image of size $M\times N$ is read as a matrix F. Let $f(x, y)$ is the gray value of the pixel located at the position (x, y), where $\{x|x=1,2,3,\ldots,M\}$ and $\{y|y=1,2,3,\ldots,N\}$. 2D multilevel thresholding image segmentation based on the 2D histogram. In order to construct the 2D histogram, the average gray value of the neighborhood of each pixel is calculated, which also be called neighborhood matrix G of the same size as F. Let $g(x, y)$ is the average gray-level value of the 3_*3 neighborhood around the pixels located at the point (x, y) and is calculated from F as follows (Ishak 2017a, b):

$$g(x,y)=\left[\frac{1}{9}\sum_{i=-1}^{1}\sum_{j=-1}^{1}f(x+i,y+j)\right] \tag{5}$$

where $[g(x, y)]$ denotes the integer part of the $g(x, y)$. We denote $V=\{v_1,\ldots,v_R\}$, $\{R|R=1,2,\ldots,256\}$ the ordered set of all average gray-levels in G (v_1 and v_R are respectively the minimum and maximum gray values). The matrix G represents the spatial correlation between the pixels in the image. The gray-level distribution and spatial gray-level distribution represented by matrices F and G, respectively are jointly used in defining the 2D histogram. To do this, the joint probability mass function matrix P of size $L\times R$ is calculated using the set U of gray values and the set V of average gray values. Theoretically, the joint probabilities $P(i, j)$ are defined as follows:

$$\begin{aligned}&P(i,j)=\text{prob}\big(f(x,y)=u_i \text{ and } g(x,y)=v_j\big),\\&\forall i=1,\ldots,L \text{ and } \forall j=1,\ldots,R\end{aligned} \tag{6}$$

In practice, $P(i, j)$ is approximated by the proportion of the image pixels with gray value ui and average gray value vj. Thus, the probabilities $P(i, j)$ defining the image 2D histogram can be calculated by:

$$P(i,j)=\frac{q\big(u_i,v_j\big)}{M\times N} \tag{7}$$

where $q(u_i, v_j)$ is the number of the image pixels with gray value u_i and average gray value v_j. $M\times N$ is the total number of pixels in the image.

2.3 Two-dimensional Tsallis entropy

The thresholding based on the 2D histogram performed better than that based on the 1D histogram. Especially, images are corrupted with noise while use of 2D histogram results in much better segmentation (Ishak 2017a, b). In the 1D multilevel thresholding method, we have only to determine m thresholds that maximize the Tsallis entropy on the 1D histogram, while 2 m values are required in the 2D multilevel thresholding approach. Indeed, we have to find m pairs of thresholding. It gives rise to the exponential increasingly when deal with more than one thresholding for the 2D multilevel thresholds. Despite this drawback, the 2D multilevel thresholding method might be effective to segment the images.

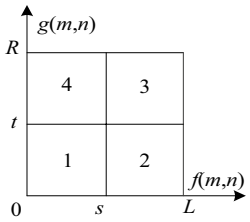

Fig. 1 2D histogram for bi-level segmentation

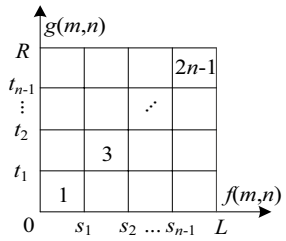

Fig. 2 2D histogram for multilevel thresholding segmentation

The 2D histogram plane is shown in Fig. 1. The histogram plane is divided into four regions by a threshold vector (s, t), where s is a threshold for original pixel and t is another threshold for the average pixel.

Regions 1 and 3 represent the object(s) and the background. Regions 2 and 4 can be ignored as the information of these two regions mostly about the edges and noises. The joint probabilities of regions 1 and 3 can be calculated by:

$$P_1(s,t)=\sum_{i=1}^{t}\sum_{j=1}^{s}P(i,j)\ ,\quad P_3(s,t)=\sum_{i=s+1}^{L}\sum_{j=t+1}^{R}P(i,j) \tag{8}$$

The 2D histogram plane can be divided into n_*n regions by the multilevel thresholds. A histogram plane with n^2 divisions is created as illustrated in Fig. 2.

The diagonal rectangles represent the object(s), intermediate region and backgrounds. Other regions are ignored which are regarded as edges and noises. Posteriori probabilities $P_1(s_1, t_1)$, $P_3(s_2, t_2)$ and $P_{2n+1}(s_n, t_n)$ can be calculated by:

$$P_1(s_1,t_1)=\sum_{i=1}^{t_1}\sum_{j=1}^{s_1}P(i,j)\ ,$$

$$P_3(s_2,t_2)=\sum_{i=s_1+1}^{s_2}\sum_{j=t_1+1}^{t_2}P(i,j) \tag{9}$$

...

$$P_{2n+1}(s_n,t_n)=\sum_{i=s_n+1}^{L}\sum_{j=t_n+1}^{R}P(i,j)$$

Therefore, the optimal 2D multilevel thresholds vector s^* and t^*, $s^*=(s_1,s_2,\ldots,s_n)$, $t^*=(t_1,t_2,\ldots,t_n)$ are obtained by maximizing the Tsallis entropy, that is:

$$T_q^{opt}(s^*,t^*)=\arg\max\left(T_q(s_1,t_1)+T_q(s_2,t_2)+\cdots+T_q(s_n,t_n)\right) \tag{10}$$

where

$$T_q(s_1,t_1)=\frac{1-\sum_{i=1}^{s_1}\sum_{j=1}^{t_1}\left(P(i,j)/P_1(s_1,t_1)\right)^q}{q-1}\ ,$$

$$T_q(s_2,t_2)=\frac{1-\sum_{i=s_1+1}^{s_2}\sum_{j=t_1+1}^{t_2}\left(P(i,j)/P_3(s_2,t_2)\right)^q}{q-1}\ ,$$

...

$$T_q(s_n,t_n)=\frac{1-\sum_{i=s_n+1}^{L}\sum_{j=t_n+1}^{R}\left(P(i,j)/P_n(s_n,t_n)\right)^q}{q-1} \tag{11}$$

3 Image segmentation based on FAGSA

3.1 Original GSA

GSA is a population-based evolutionary algorithm inspired by the concept of gravity (Rashedi et al. 2009). The GSA is based on the law of universal gravitation that all the objects in the universe are attracted to each other by the gravity force, this force causes a global movement of all objects, and small mass objects are approaching to big mass objects. The mass and distance affects the gravitational force. Therefore, there is a great potential in this field to adopt the gravity concept in producing effective search operators. The detail process of the GSA is described as follows. Now, consider a system with N agents (masses), the position of the ith agent is defined by:

$$X_i=\left(x_i^1,\ldots,x_i^d,\ldots,x_i^n\right),\quad i=1,\ 2,\ \ldots,N \tag{12}$$

where x_i^d is the position of the ith agent in the dth dimension and n is the dimension of the population.

Mass of each agent i is calculated according to its current objective function as follows:

$$m_i(t)=\frac{fit_i(t)-worst(t)}{best(t)-worst(t)} \tag{13}$$

$$M_i(t)=\frac{m_i(t)}{\sum_{j=1}^{N}m_j(t)} \tag{14}$$

where $M_i(t)$ and $fit_i(t)$ represent the mass and the fitness value of the agent i at generation t, respectively. For a maximization problem, worst(t) and best(t) are defined as follows:

$$\begin{aligned}best(t)&=\max fit_i(t)\\worst(t)&=\min\ fit_i(t)\end{aligned} \tag{15}$$

In order to calculate the acceleration of an agent, the total forces from a set of heavier masses that apply on an agent based on the modified law of gravity, which is measured by follow formulas:

$$F_i^d(t)=\sum_{j\in kbest,i\neq j}rand_jF_{ij}^d(t) \tag{16}$$

$$F_{ij}^d(t)=G(t)\frac{M_{pi}(t)M_{aj}(t)}{R_{ij}+\varepsilon}\left(x_j^d(t)-x_i^d(t)\right) \tag{17}$$

where $M_{ai}(t)$ is the active gravitational mass related to agent j, $M_{pi}(t)$ is the passive gravitational mass related to agent i which can calculate by Eqs. (13) and (14), $rand_j$ is uniform random values in the interval [0,1], ε is a small value, and $R_{ij}$is the distance between the two agents i and j. $kbest$ is the set of first k agents with the best fitness values and biggest masses. Especially, $G(t)$ is gravitational constant which will decrease with time, the corresponding equation is given by:

$$G(t)=G_0*e^{\frac{-\alpha t}{T}} \tag{18}$$

where G_0 are the constant and α is the damping factor. The acceleration now can be expressed as:

$$a_i^d(t)=\frac{F_i^d(t)}{M_{ii}(t)} \tag{19}$$

where $M_{ii}(t)$ is the inertia mass of ith agent, which also can compute by Eqs. (13) and (14). Then the next velocity of an agent i satisfies the follow expression:

$$v_i^d(t+1)=rand_i*v_i^d(t)+a_i^d(t) \tag{20}$$

where $rand_i$ is uniform random values in the interval [0,1]. In order to better control the next velocity, an inertia weight is taken into account, therefore the Eq. (20) can be modified by

$$v_i^d(t+1)=\omega(t+1)*rand_i*v_i^d(t)+a_i^d(t) \tag{21}$$

Then, the agent's next position can be updated by follow equation:

$$x_i^d(t+1) = x_i^d(t) + v_i^d(t+1) \tag{22}$$

A better representation of the GSA process is shown in Fig. 3.

3.2 FAGSA

In generally, it is probably impossible to define a unique set of parameters that work well in all cases. However, the following FAGSA has been useful to work in practice. According to the analysis, it is known that.

1. When searching the best fitness at the end of run, low inertia weight and low gravitational constant are often preferred.
2. When the best fitness has been stayed at one value for a long time, simply increasing the number of iterations does not work. The inertia weight and gravitational constant should be increased.

Therefore, a fuzzy system is utilized to adaptive control the inertia weight and gravitational constant with the best fitness (*BF*) and the number of iteration which the best fitness value is unchanged (*NU*) as the input variables, and the inertia weight (ω) and control parameter (α) as the output variables. The normalized best fitness (*NBF*) in the range of [0, 1] can be calculated by follow:

$$NBF = \frac{BF - BF_{\min}}{BF_{\max} - BF_{\min}} \tag{23}$$

where $BF_{\min}$ and $BF_{\max}$ are the estimated minimum and maximum values of best fitness. *NU* values are normalized in a similar way. The bound values for ω and α are $0.2 \le \omega \le 1.2$, $10 \le \alpha \le 50$.

The membership functions of every input and output are shown in Fig. 4. The fuzzy important rules of the inertia weight (ω) and control parameter (α) were shown in Table 1. According to Table 1, PS (positive small), PM (positive medium) and PB (positive big) are the linguistic values for all of the input and output variables. According to the above description, the flow chart of the proposed FAGSA is shown in Fig. 5.

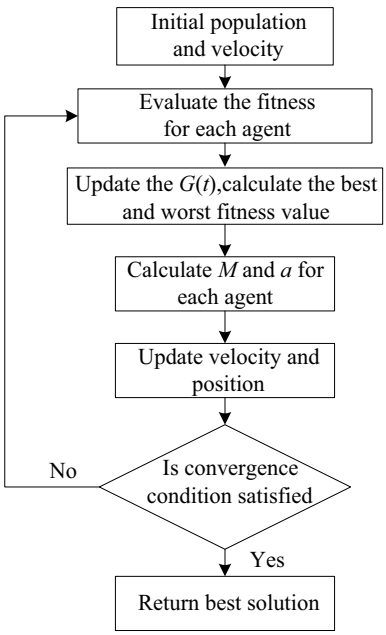

Fig. 3 General principle of the GSA

4 Experiments

In this section, the performance of the proposed algorithm was evaluated. Firstly, the test images and the algorithms used in the comparison were introduced in Sect. 4.1, followed by the detailed results on the objective function value shown in Sect. 4.2. Then, two popular measure metrics were used to verify the segmentation performance in Sect. 4.3. Finally, the application of the four algorithms was given in Sect. 4.4.

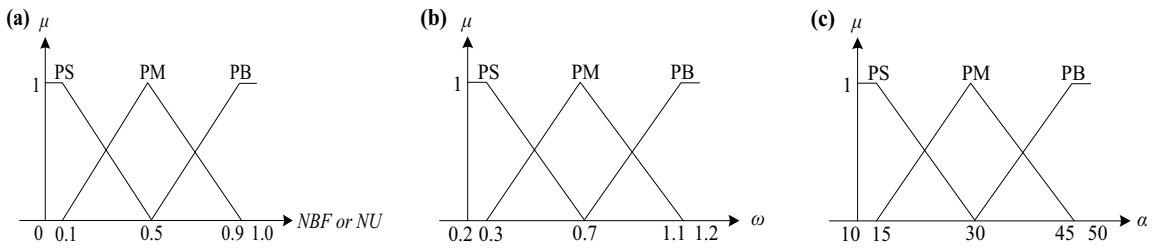

Fig. 4 Membership functions of inputs and outputs. **a** *NBF* or *NU*, **b** ω, and α

Table 1 Fuzzy rules for the inertia weight ω and the control parameter α

ω		*NU*			α		*NU*		
		PS	PM	PB			PS	PM	PB
NBF	PS	PS	PM	PB	*NBF*	PB	PS	PM	PS
	PM	PM	PM	PB		PM	PM	PM	PS
	PB	PM	PB	PB		PB	PM	PS	PS

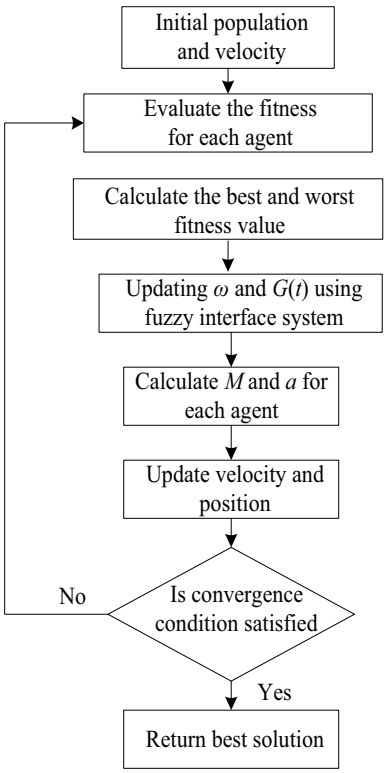

Fig. 5 General principle of the FAGSA

4.1 Experiment set up

The proposed algorithm used two-dimension Tsallis entropy as its objective function will be tested under a set of benchmark images. The test images named 'Lena', 'Goldhill', 'Lake' and 'Butterfly', and the size of the images are 512×512. The original images and corresponding histograms are shown in Fig. 6. We can find that the 2D histograms are multimodal. Therefore, the test images are suitable for multilevel thresholding image segmentation.

The experiments were carried out on a PC with an Intel Corei7 processor and 8 GB memory. The global optimization toolbox of MATLAB R2018a runs on windows ten system. The DE, PSO and GSA are implemented under the same conditions. Generally, the experiments test thresholding are $m = 2, 3, 4, 5$. All population individuals were uniformly randomly initialized within [0, 255]. The number of iteration set to 300 in per experiment and the population size set to 30. Besides, all the experiments were repeated 30 times. The corresponding parameters used for the presented four algorithms are listed in Table 2.

4.2 Results on the objective function

As the aim of the multilevel thresholding is to maximize the given objective function, the objective function value obtained by the involved algorithms directly shows the algorithm's performance. In detail, the mean and standard deviation of objective function values are shown in Table 3.

As shown in Table 3, it can be observed that all the test images with different algorithms show relatively high objective function values. Obviously, as the increase of the number of the threshold, the four algorithms can get high objective function values. Generally, the FAGSA outperform the other three algorithms, DE and PSO show similar objective functions, while GSA is a little inferior. Besides, from the perspective of standard deviation of the objective function values, the FAGSA shows obviously advantages over DE, PSO and GSA. The smaller the standard deviation is, the smaller the change of objective functions over the course of iterations will be, that is, the better stability of segmentation. Therefore, the results show that the FAGSA obtains exciting effect in stability.

4.3 Quality measure and time consumption of segmented image

To verify the performance of the proposed algorithm, the time consumption and appropriate performance indicator peak signal noise ratio (PSNR) were calculated to evaluate the corresponding image segmentation quality. Image quality measurement using peak signal to noise ratio (PSNR) is defined as (Horng 2011):

$$PSNR = 20 \log_{10}\left(\frac{255}{RMSE}\right), \quad (dB) \tag{24}$$

where

$$RMSE = \sqrt{\frac{\sum_{i=1}^{M}\sum_{j=1}^{N}(I(i,j) - C(i,j))^2}{M \times N}} \tag{25}$$

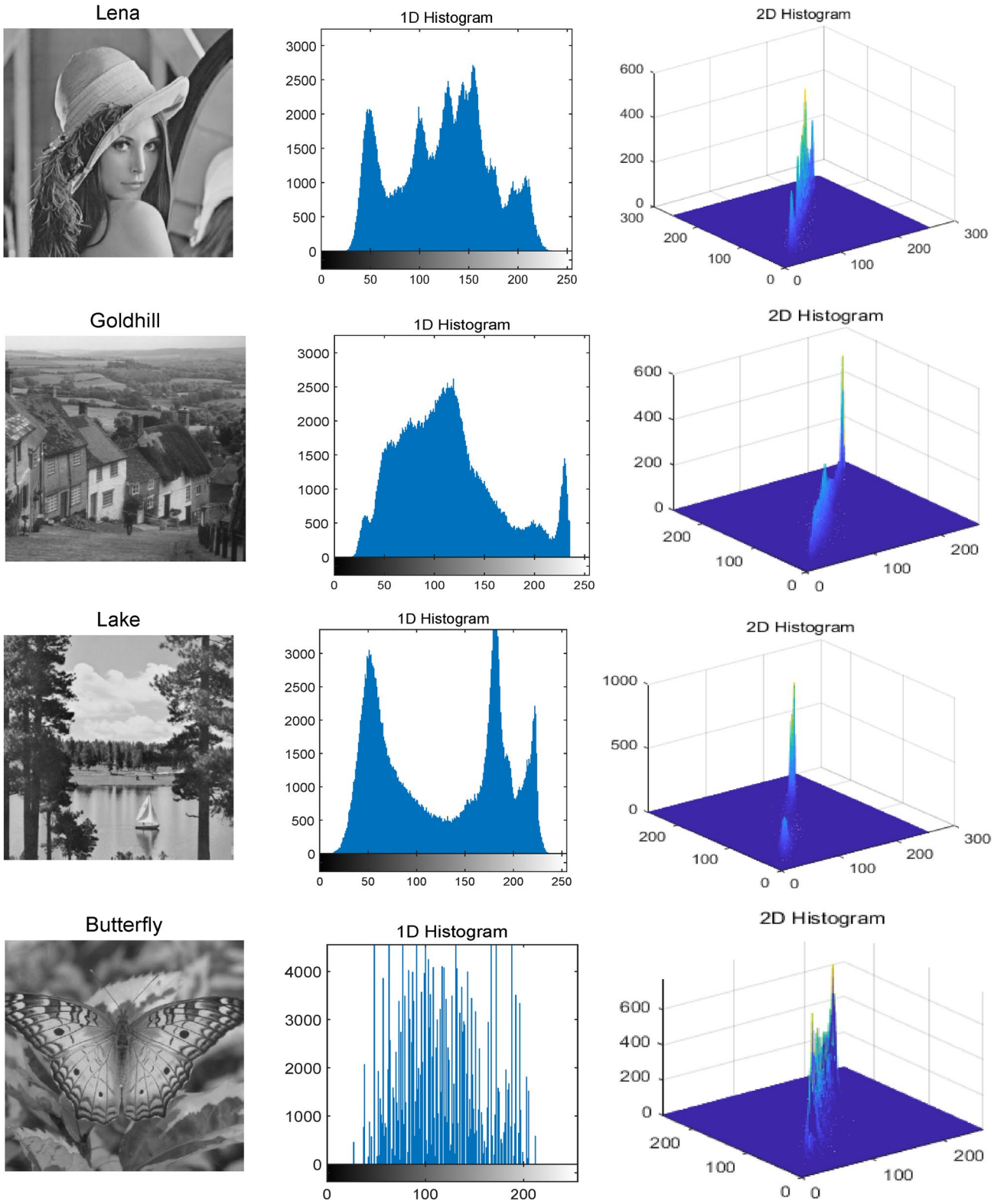

Fig. 6 The test images and their histograms

Table 2 Parameters of the four algorithms

Algorithms	Parameters	Value
DE	Crossover probability (CR)	0.8
	Mutation probability (F)	0.5
PSO	Maximum speed (v_{max})	2
	Inertia weight (ω)	0.5
	Accelerated factor ($c_1 = c_2$)	2
	Rand number (r_1, r_2)	[0, 1]
GSA	Constant (G_0)	100
	Inertia weight (ω)	0.6
	Control parameter (α)	30
FAGSA	Constant (G_0)	100
	The bound values for (ω)	$0.2 \le \omega \le 1.2$
	The bound values for (α)	$10 \le \alpha \le 50$

Table 4 displays the PSNR metric and time consumption of the test images segmented with different thresholds by the four algorithms. The results show FAGSA achieves the highest assessment, testifying to the superiority of FAGSA. However, PSNR values do not increase as the number of thresholds increases, when the number of the thresholding is three, the PSNR get the maximum values, expect the test image 'Lake'. It demonstrates that the number of 2D multilevel thresholds is not the more the better. Therefore, the selection of appropriate thresholds number needs to be based on the 2D histogram. Compared to the computation time of the four algorithms, the FAGSA is better than the other algorithms. It can be observed that FAGSA demonstrates better time efficiency and excellent segmentation results and has obvious advantages, especially over GSA in computation time. Therefore, it can be safely assumed that FAGSA is a desirable image segmentation method with high efficiency and of high quality.

4.4 Comparing the performance in noisy image segmentation

In this Section, we present a comparative study with the other three multilevel thresholding segmentation algorithms. The objective is to highlight the effectiveness of the FAGSA. The images corrupted by Gaussian noise and salt and pepper noise are considered to perform the contrast experiment. In the experiment, the mean value and variance of the two noises are set to 0 and 0.02, respectively. Besides, we set the number of the thresholds to three for the 2D multilevel thresholding. Figures 7 and 8 illustrate the segmentation results obtained by the competitive approaches on the different noisy images. Visually, these experimental results show that the images segmented by the FAGSA are more clearly and with higher veracity. Indeed, we observe that the FAGSA for 2D multilevel thresholding achieves a good balance between smooth borders, preserving image details and robustness to different types and levels of noise. This effectiveness is much more remarkable on the multimodal images. To make the experimental results more convincing, we choose two popular measures SSIM and FSIM index to support our claim (Agrawal et al. 2013).

The SSIM is used to access the similarity of the original and segmented image. The SSIM index is defined as:

Table 3 Comparison of the mean and standard deviation of objective function values

Test images	m	The mean of objective function values				The standard of objective function values			
		GSA	PSO	DE	FAGSA	GSA	PSO	DE	FAGSA
Lena	2	44.5514	44.5647	44.5584	44.7759	0.0557	0.0443	0.0498	0.0415
	3	53.8439	54.3775	54.3551	54.3799	0.0891	0.0672	0.0687	0.0445
	4	63.1018	62.4083	63.1073	66.7963	0.1103	0.9512	0.0751	0.0638
	5	70.9596	70.944	70.8112	70.673	0.1447	0.1564	0.1245	0.0812
Goldhill	2	47.8502	48.5148	48.4241	48.5209	0.0611	0.0404	0.0527	0.0382
	3	58.2418	58.5488	58.1974	58.287	0.0727	0.0655	0.0511	0.0451
	4	67.7229	67.7475	67.5879	67.9007	0.1008	0.0842	0.0729	0.0622
	5	76.2626	76.3989	76.4789	76.5107	0.1299	0.1103	0.1025	0.0743
Lake	2	50.1256	50.3678	50.3661	50.3678	0.0162	0.0122	0.0152	0.0029
	3	61.6397	61.6371	61.6442	61.6157	0.0354	0.0275	0.0286	0.0255
	4	70.1241	70.5854	70.1241	70.5103	0.0645	0.0488	0.0518	0.0461
	5	79.0205	79.0351	79.2053	78.9958	0.0946	0.0734	0.0753	0.0663
Butterfly	2	40.0137	40.4382	40.6401	40.7225	0.0334	0.0251	0.0175	0.0132
	3	48.6767	48.7347	49.299	49.7667	0.0566	0.0314	0.0116	0.0064
	4	56.7068	56.4886	55.5653	55.3844	0.0683	0.0375	0.0364	0.0351
	5	60.4305	63.0306	59.6499	62.3029	0.0757	0.0564	0.0681	0.0462

Table 4 Comparison of the mean PSNR and Time consumption

Test images	m	PSNR				Computation time (s)			
		GSA	PSO	DE	FAGSA	GSA	PSO	DE	FAGSA
Lena	2	16.0754	16.2307	16.116	17.0756	1.6432	1.3982	1.0584	0.6534
	3	17.7133	18.0979	18.1722	18.238	3.1302	2.4316	1.7382	1.2791
	4	16.9199	15.9466	16.981	17.6059	4.5196	3.626	2.4498	1.8918
	5	15.7662	15.6266	15.6581	16.712	6.1024	4.7306	3.125	2.4356
Goldhill	2	16.9866	17.1196	17.0294	17.2308	1.663	1.3228	0.9912	0.5917
	3	17.3536	16.6962	17.2851	17.4348	2.8476	2.4716	1.775	1.1974
	4	16.0034	16.4154	16.2911	16.5062	4.3914	3.6454	2.5931	1.7932
	5	15.9785	15.5081	15.422	15.4711	5.9308	4.6508	2.0478	2.7541
Lake	2	17.0016	17.2894	17.2843	17.2894	1.4356	1.3843	1.0051	0.1715
	3	15.7739	16.2457	15.8691	16.4812	2.9382	2.5586	1.7289	1.2654
	4	15.521	15.7269	15.5106	15.8781	4.7492	3.6308	2.6485	1.6536
	5	15.0473	15.1471	15.0469	15.3206	6.0484	4.8996	3.0918	2.3758
Butterfly	2	16.3773	16.2899	16.4565	16.5805	1.4682	1.379	1.0526	0.6429
	3	16.8915	16.7699	16.6823	16.9735	2.7686	2.5156	1.6432	1.1352
	4	14.8635	14.5414	14.5961	16.3461	4.5294	3.9368	2.5342	1.5837
	5	13.6998	13.7851	14.9926	14.9062	5.9026	4.8224	3.3424	1.8569

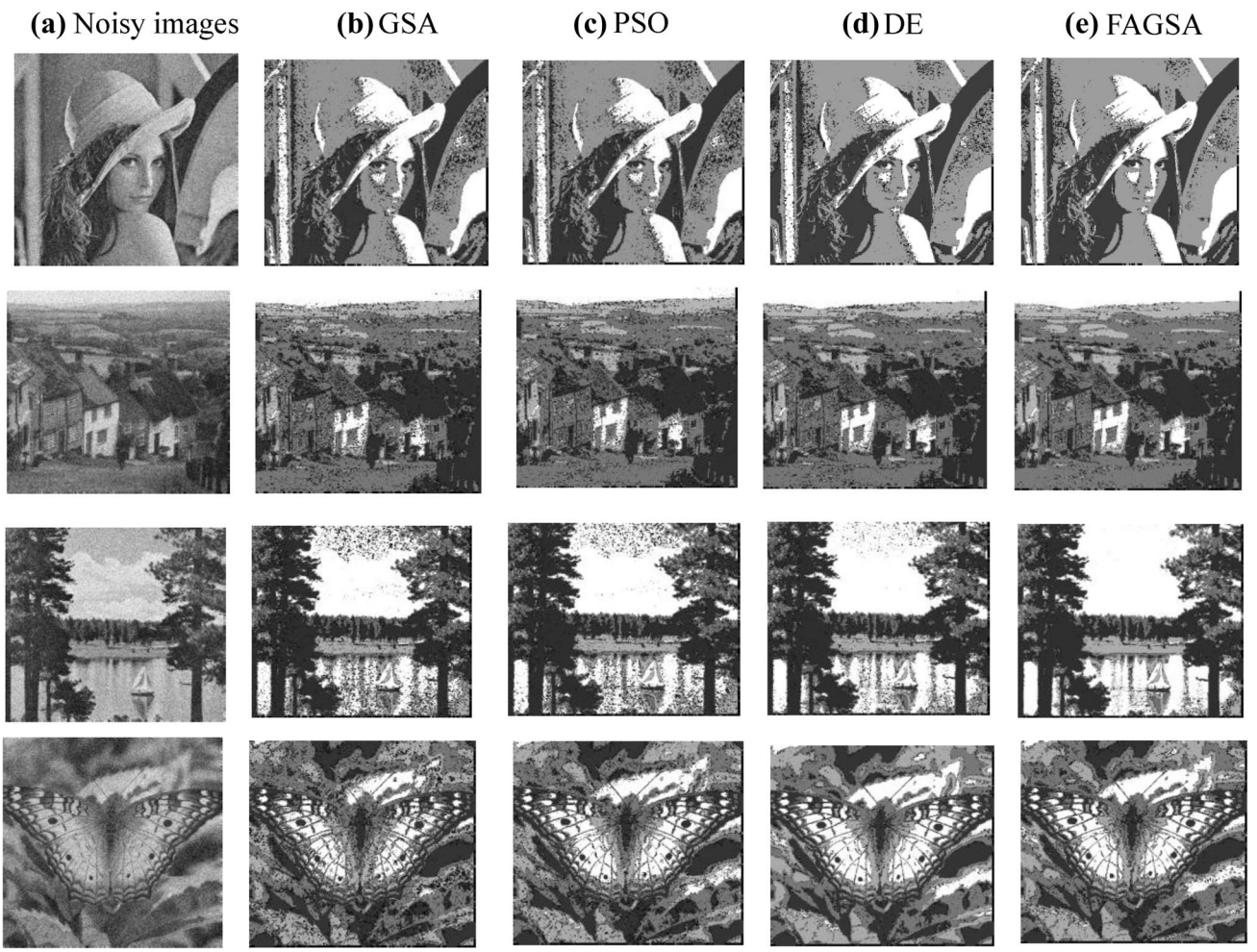

Fig. 7 Segmentation results on test images corrupted by Gaussian noise

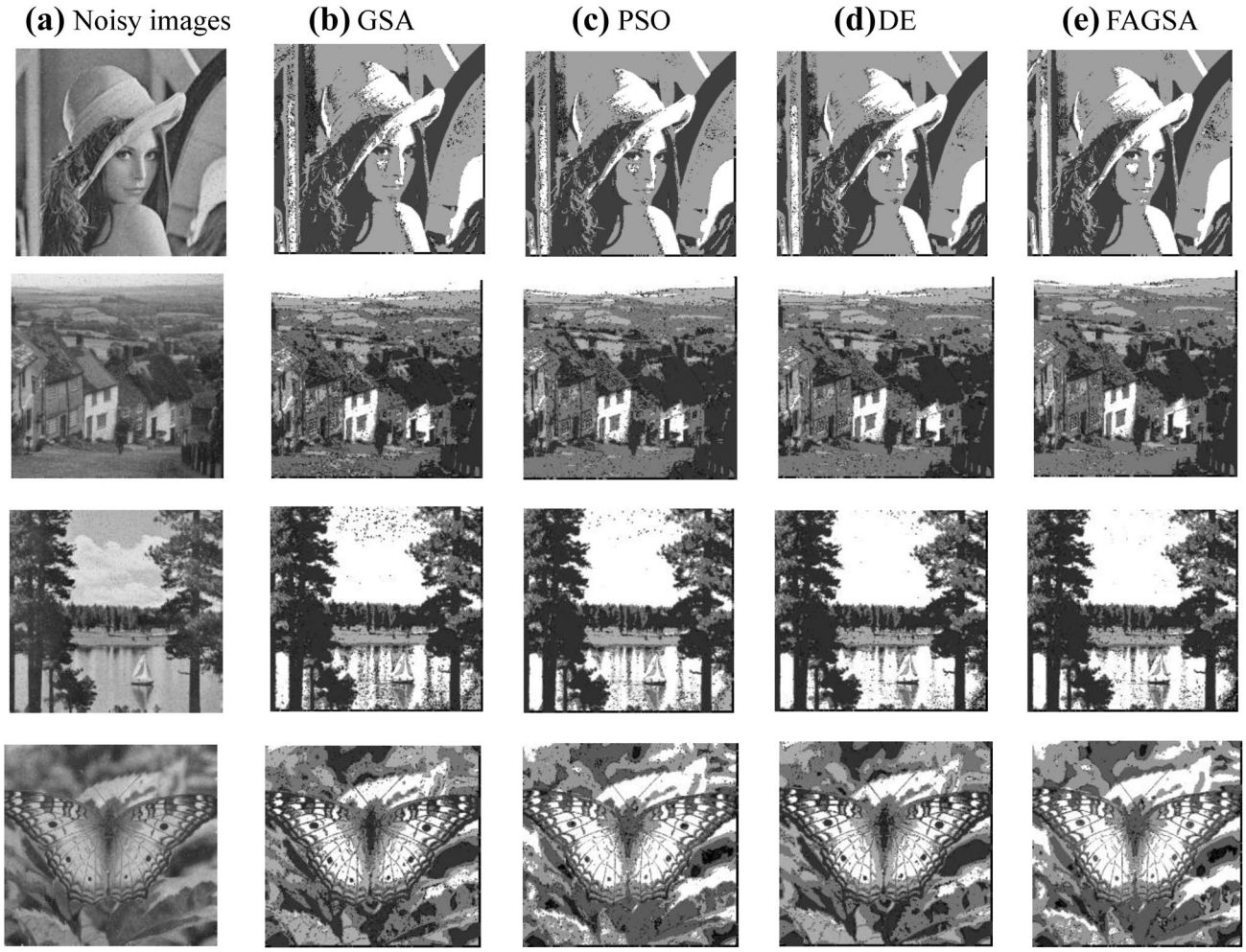

Fig. 8 Segmentation results on test images corrupted by salt and pepper noise

$$SSIM(C,I) = \frac{\left(2\mu_C\mu_I + C_1\right)\left(2\delta_{CI} + C_2\right)}{\left(\mu_C^2 + \mu_I^2 + C_1\right)\left(\delta_C^2 + \delta_I^2 + C_2\right)} \tag{26}$$

where μ_C, δ_C respectively represent the pixel mean and variance of original image. μ_I, δ_I respectively represent the pixel mean and variance of segmented image. δ_{CI} is the covariance of the original image and the segmented image. C_1, C_2 are the constant, here, $C_1 = C_2 = 6.5025$. The highest value of SSIM shows a better performance. In addition, the FSIM is employed to measure the feature similarity between two images. It is calculated between two images C and I as:

$$FSIM = \frac{\sum_{x\in\Omega} S_L(x)PC_m(x)}{\sum_{x\in\Omega} PC_m(x)} \tag{27}$$

where

$$\begin{aligned} S_L(x) &= S_{PC}(x)S_G(x);\\ S_{PC}(x) &= \frac{2PC_1(x)PC_2(x) + T_1}{PC_1^2(x) + PC_2^2(x) + T_1};\\ S_G(x) &= \frac{2G_1(x)G_2(x) + T_2}{G_1^2(x) + G_2^2(x) + T_2};\\ PC_m(x) &= \max\left\{PC_1(x), PC_2(x)\right\}. \end{aligned} \tag{28}$$

And, T_1 and T_2 are constants. Here, we choose $T_1 = 0.85$ and $T_2 = 160$ in the experiments, $G(x)$ represents the gradient magnitude of an image, $PC(x)$ is the phase congruence of an image. A higher value of FSIM indicates better performance. The experimental data are shown in Tables 5 and 6. The results indicate the FAGSA perform better than the other three algorithms, which are consistent with the visual analysis. In conclusion, the proposed algorithm achieved significant improvements based on the original GSA; and when compared with other meta-heuristic algorithms, the proposed algorithm

Table 5 Comparison of the SSIM and FSIM with Gaussian noise

Noisy images	SSIM				FSIM			
	GSA	PSO	DE	FAGSA	GSA	PSO	DE	FAGSA
Lena	0.0633	0.0688	0.0834	0.1076	0.6172	0.622	0.6351	0.6466
Goldhill	0.063	0.0705	0.0861	0.1067	0.6928	0.7124	0.7392	0.7561
Lake	0.1131	0.1242	0.1373	0.1912	0.6923	0.7225	0.7413	0.7598
Butterfly	0.0879	0.1104	0.1252	0.1469	0.6932	0.6961	0.7184	0.7344

Table 6 Comparison of the SSIM and FSIM with salt and pepper noise

Noisy images	SSIM				FSIM			
	GSA	PSO	DE	FAGSA	GSA	PSO	DE	FAGSA
Lena	0.1109	0.1204	0.1331	0.1563	0.6235	0.6324	0.64	0.6612
Goldhill	0.1097	0.1402	0.1611	0.1944	0.7169	0.7246	0.7271	0.7352
Lake	0.1885	0.2148	0.2345	0.2606	0.7351	0.7703	0.78	0.7954
Butterfly	0.1795	0.1806	0.2023	0.2176	0.7066	0.7136	0.7257	0.7429

offered stability in 2D multilevel image thresholding and better image segmentation quality.

5 Conclusions

In this paper, we proposed an improved GSA, called the FAGSA, for 2D multilevel thresholds selection using Tsallis entropy. In the FAGSA, a fuzzy system is designed for intelligently updating the inertia weight (ω) and control parameter (α) to realize adaptive selection of parameters for different optimization problems. The experiments demonstrated the effectiveness of the FAGSA. In the experiments, the proposed algorithm in comparison with DE, PSO and GSA in 2D multilevel thresholds image segmentation. The experimental results demonstrate the superiority of our algorithm in terms of the objective function value, image quality measures and time consumption. Future works of this study will focus on studying the performance of the proposed algorithm on remote sensing images.

Acknowledgements This work is supported by GDAS' Project of Science and Technology Development (2019GDASYL- 0103077, 2018GDASCX-0115, 2017GDASCX-0115).

References

Abdel-Khalek S, Ishak AB, Omer OA et al (2017) A two-dimensional image segmentation method based on genetic algorithm and entropy[J]. Optik 131:414–422

Agrawal S, Panda R, Bhuyan S et al (2013) Tsallis entropy based optimal multilevel thresholding using cuckoo search algorithm[J]. Swarm Evol Comput 11:16–30

Badrinarayanan V, Kendall A, Cipolla R (2017) Segnet: a deep convolutional encoder-decoder architecture for image segmentation[J]. IEEE Trans Pattern Anal Mach Intell 39(12):2481–2495

Beigvand SD, Abdi H, La Scala M (2016) Combined heat and power economic dispatch problem using gravitational search algorithm[J]. Electr Power Syst Res 133:160–172

Bhandari AK, Singh VK, Kumar A et al (2014) Cuckoo search algorithm and wind driven optimization based study of satellite image segmentation for multilevel thresholding using Kapur's entropy[J]. Expert Syst Appl 41(7):3538–3560

Bhandari AK, Kumar A, Singh GK (2015) Modified artificial bee colony based computationally efficient multilevel thresholding for satellite image segmentation using Kapur's, Otsu and Tsallis functions[J]. Expert Syst Appl 42(3):1573–1601

Bhandari AK, Kumar A, Chaudhary S et al (2016) A novel color image multilevel thresholding based segmentation using nature inspired optimization algorithms[J]. Expert Syst Appl 63:112–133

Chen LC, Papandreou G, Kokkinos I et al (2017) Deeplab: Semantic image segmentation with deep convolutional nets, atrous convolution, and fully connected crfs[J]. IEEE Trans Pattern Anal Mach Intell 40(4):834–848

Cheriet M, Said JN, Suen CY (1998) A recursive thresholding technique for image segmentation[J]. IEEE Trans Image Process 7(6):918–921

Doraghinejad M, Nezamabadi-pour H (2014) Black hole: a new operator for gravitational search algorithm. Int J Comput Intell Syst 7(5):809–826

Duman S, Güvenç U, Sönmez Y et al (2012) Optimal power flow using gravitational search algorithm[J]. Energy Convers Manage 59:86–95

El Aziz MA, Ewees AA, Hassanien AE (2017) Whale optimization algorithm and moth-flame optimization for multilevel thresholding image segmentation[J]. Expert Syst Appl 83:242–256

Erwin S, Saputri W (2018) Hybrid multilevel thresholding and improved harmony search algorithm for segmentation[J]. Int J Electr Comput Eng (IJECE) 8(6):4593–4602

Gandomi AH, Yang XS, Alavi AH et al (2013) Bat algorithm for constrained optimization tasks[J]. Neural Comput Appl 22(6):1239–1255

Han X, Chang X (2012) A chaotic digital secure communication based on a modified gravitational search algorithm filter. Inf Sci 208:14–27

He L, Huang S (2017) Modified firefly algorithm based multilevel thresholding for color image segmentation[J]. Neurocomputing 240:152–174

Horng MH (2011) Multilevel thresholding selection based on the artificial bee colony algorithm for image segmentation[J]. Expert Syst Appl 38(11):13785–13791

Ishak AB (2017a) A two-dimensional multilevel thresholding method for image segmentation[J]. Appl Soft Comput 52:306–322

Ishak AB (2017b) Choosing parameters for Rényi and Tsallis entropies within a two-dimensional multilevel image segmentation framework[J]. Phys A 466:521–536

Kang K, Bae C, Yeung HWF et al (2018) A hybrid gravitational search algorithm with swarm intelligence and deep convolutional feature for object tracking optimization[J]. Appl Soft Comput 66:319–329

Khairuzzaman AKM, Chaudhury S (2017) Multilevel thresholding using grey wolf optimizer for image segmentation[J]. Expert Syst Appl 86:64–76

Kumar Y, Sahoo G (2014) A review on gravitational search algorithm and its applications to data clustering & classification[J]. Int J Intell Syst Appl 6(6):79

Li K, Tan Z (2019) An improved flower pollination optimizer algorithm for multilevel image thresholding[J]. IEEE Access 7:165571–165582

Nagpal S, Arora S, Dey S (2017) Feature selection using gravitational search algorithm for biomedical data[J]. Procedia Comput Sci 115:258–265

Nobahari H, Nikusokhan M, Siarry P (2012) A multi-objective gravitational search algorithm based on non-dominated sorting. Int J Swarm Intell Res 3(3):32–49

Pare S, Bhandari AK, Kumar A et al (2018) A new technique for multilevel color image thresholding based on modified fuzzy entropy and Lévy flight firefly algorithm[J]. Comput Electr Eng 70:476–495

Raja NSM, Fernandes SL, Dey N et al (2018) Contrast enhanced medical MRI evaluation using Tsallis entropy and region growing segmentation[J]. J Ambient Intell Human Comput. https://doi.org/10.1007/s12652-018-0854-8

Rashedi E, Nezamabadi-Pour H (2013) A stochastic gravitational approach to feature based color image segmentation[J]. Eng Appl Artif Intell 26(4):1322–1332

Rashedi E, Nezamabadi-Pour H, Saryazdi S (2009) GSA: a gravitational search algorithm[J]. Inf Sci 179(13):2232–2248

Rashedi E, Rashedi E, Nezamabadi-pour H (2018) A comprehensive survey on gravitational search algorithm[J]. Swarm and Evolut Comput 41:141–158

Sarafrazi S, Nezamabadi-pour H, Seydnejad SR (2015) A novel hybrid algorithm of GSA with Kepler algorithm for numerical optimization[J]. J King Saud Univ-Comput Inf Sci 27(3):288–296

Sarkar S, Das S, Chaudhuri SS (2015) A multilevel color image thresholding scheme based on minimum cross entropy and differential evolution[J]. Pattern Recogn Lett 54:27–35

Sha C, Hou J, Cui H (2016) A robust 2D Otsu's thresholding method in image segmentation[J]. J Vis Commun Image Represent 41:339–351

Sun G, Zhang A, Jia X et al (2016) DMMOGSA: Diversity-enhanced and memory-based multi-objective gravitational search algorithm[J]. Inf Sci 363:52–71

Sun G, Ma P, Ren J et al (2018) A stability constrained adaptive alpha for gravitational search algorithm[J]. Knowl-Based Syst 139:200–213

Xiong L, Chen R, Zhou X et al (2019a) Multi-feature fusion and selection method for an improved particle swarm optimization[J]. J Ambient Intell Human Comput. https://doi.org/10.1007/s12652-019-01624-4

Xiong L, Zhang D, Li K et al (2019b) The extraction algorithm of color disease spot image based on Otsu and watershed[J]. Soft Comput. https://doi.org/10.1007/s00500-019-04339-y

Yazdani S, Nezamabadi-pour H, Kamyab S (2014) A gravitational search algorithm for multimodal optimization[J]. Swarm Evolut Comput 14:1–14

Zeng N, Wang Z, Zhang H et al (2016) Deep belief networks for quantitative analysis of a gold immunochromatographic strip[J]. Cogn Comput 8(4):684–692

Zeng N, Qiu H, Wang Z et al (2018) A new switching-delayed-PSO-based optimized SVM algorithm for diagnosis of Alzheimer's disease[J]. Neurocomputing 320:195–202